Mercury emission from a temperate lake during autumn turnover

Jennifer L. Wollenberg, Stephen C. Peters*

Department of Earth and Environmental Sciences, Lehigh University, Bethlehem PA, USA

ABSTRACT

Lakes in temperate regions stratify during summer and winter months, creating distinct layers of water differentiated by their physical and chemical characteristics. When lakes mix in autumn and spring, mercury cycling may be affected by the chemical changes that occur during mixing. Sampling was conducted in Lake Lacawac, Eastern Pennsylvania, USA, throughout the autumn of 2007 to characterize changes in emission of gaseous elemental mercury (Hg^0) from the lake surface and dissolved mercury profiles in the water column during mixing. Water chemistry and weather parameters were also measured, including dissolved organic carbon (DOC), iron, and solar radiation which have been shown to interact with mercury species. Results indicate that emission of Hg^0 from the lake to the atmosphere during turnover was controlled both by solar radiation and by surface water mercury concentration. As autumn turnover progressed through the months of October and November, higher mercury concentration water from the hypolimnion mixed with epilimnetic water, increasing mercury concentration in epilimnetic waters. Dissolved absorbance was significantly correlated with mercury concentrations and with iron, but DOC concentrations were essentially constant throughout the study period and did not exhibit a relationship with either dissolved mercury concentrations or emission rates. Positive correlations between dissolved mercury and iron and manganese also suggest a role for these elements in mercury transport within the lake, but iron and manganese did not demonstrate a relationship with emission rates. This research indicates that consideration of seasonal processes in lakes is important when evaluating mercury cycling in aquatic systems.

1.   Introduction

Mercury in aquatic systems bioaccumulates in the food web and has toxic effects at all trophic levels. The reduction of dissolved Hg(II) to Hg^0 often results in partitioning of mercury from terrestrial or aquatic surfaces to the atmosphere (Lindberg et al., 1998; Morel et al., 1998), and is one pathway for removal of mercury from the water column, thereby decreasing the amount available for methylation and bioaccumulation. Many natural waters are oversaturated with dissolved gaseous mercury (DGM) with respect to the atmosphere (Vandal et al., 1991), generating a concentration gradient from the water to the air. The resultant flux of Hg^0 from the water surface, as measured using the dynamic flux chamber method described by Carpi and Lindberg (1998), can be calculated using the following equation:

$$J_{Hg} = (C_i - C_o)\left(\frac{Q}{A}\right) \qquad (1)$$

where J_{Hg} is the calculated mercury flux, Q is the air sampling flow rate, A is the water surface area within the chamber, and

* Corresponding author.
  E-mail address: scp2@lehigh.edu (S.C. Peters).

C_i and C_o are the chamber and ambient mercury concentrations, respectively.

Interactions between aqueous mercury species and solar radiation can cause both photooxidation ($Hg^0 \rightarrow Hg(II)$), which may reduce emission, and photoreduction ($Hg(II) \rightarrow Hg^0$), which may increase emission (Amyot et al., 1997a; Lalonde et al., 2001). The wavelengths of light responsible for these processes include UV-A, UV-B, and visible light. Studies in high DOC lakes have found that visible wavelengths exert the strongest influence on Hg^0 formation (Amyot et al., 1997c), in contrast to lower DOC systems where ultraviolet wavelengths appear to be most important (Amyot et al., 1997b; Garcia et al., 2005). These findings suggest that wavelength dependence may vary depending on DOC concentration, quality, and water transparency. The process of mercury reduction is coupled to the photooxidation of DOC (Amyot et al., 1997a; Garcia et al., 2005; Tseng et al., 2004). Mercury–DOC interactions are dependent on pH and DOC characteristics (Haitzer et al., 2003), as well as competitive effects with other dissolved constituents such as sulfide (e.g. Reddy and Aiken, 2001). Observed relationships between total dissolved mercury and DOC, iron, and manganese in the hypolimnion of lakes suggest that these elements may play an important role in mercury transport (Chadwick et al., 2006). Increased production of Hg^0 in the presence of Fe(III) implies that mercury emission may be enhanced in iron-enriched surface waters (Zhang and Lindberg, 2001).

Mercury, DOC, iron, and manganese cycles may be influenced by seasonal changes in the physical and chemical properties of lake water. In temperate regions of the globe, the development of seasonal lake stratification driven by water temperature gradients during summer and winter months results in the development of distinct layers of water differentiated by their physical (temperature, density) and chemical (pH, oxygenation, redox status) characteristics. Mercury can become enriched in hypolimnetic waters where dissolved oxygen is low (Herrin et al., 1998; Slotton et al., 1995; Watras and Bloom, 1994). When lake mixing occurs in autumn and spring, pH, redox status, and oxygen saturation become uniform throughout the water column resulting in dramatic changes in the water chemistry that will affect the speciation of mercury, iron, and other dissolved constituents. Total dissolved mercury concentrations in both hypolimnetic and epilimnetic waters were elevated before turnover in a Wisconsin lake and decreased after turnover (Herrin et al., 1998). Mercury emission was not quantified, but it is possible that the net decrease in dissolved mercury could be explained by mercury loss to the atmosphere during destratification (Herrin et al., 1998).

In this research, we seek to determine whether physical and chemical changes in the water column during lake turnover alter the rate of mercury emission to the atmosphere. Since iron has been shown to be important in controlling the formation of Hg^0 in freshwater systems (Zhang and Lindberg, 2001), it is reasonable to suggest that emission rates from freshwater lakes may increase during autumn turnover when anoxic, iron-rich bottom water mixes with more oxic waters from the epilimnion. Conversely, seasonal declines in solar radiation are likely to limit emission. Production of Hg^0 is driven by the solar photon flux with higher Hg(II) to Hg^0 reduction rates observed in spring and summer (Zhang et al.,

2006). In this paper, we report on a 3 month long experiment designed to test how these factors influence mercury emission rates during autumn turnover. Paired water sampling and emission measurements were conducted in a freshwater lake during the time period when mixing was expected.

1.1. Study site

Lake Lacawac is located in the Pocono Mountains of northeastern Pennsylvania, U.S.A. (41.3821N, 75.2916W; Fig. 1). This and other lakes in the Northeastern United States have been subject to atmospheric deposition of mercury sourced primarily from fossil fuel combustion facilities to the west. Previous studies of this lake have shown the development of anoxia during summer stratification, seasonal changes in DOC chemical characteristics, and have suggested that dissolved iron concentrations vary based on the degree of stratification and anoxia (Maloney et al., 2005).

2. Experimental

2.1. Mercury emission measurements and water sample collection

Water temperature was continuously measured at 1 m depth intervals throughout the study period using temperature probes suspended from a floating dock at the center of the lake to monitor changes in lake stratification on a daily basis. Temperature data were used to characterize location of the thermocline and the extent to which the lake destratified during the autumn months. Mercury emission measurements and lake water sampling were conducted while the lake was strongly stratified, in early September. During the autumn destratification, mercury samples were obtained on five additional dates throughout the months of September, October and November. The final sampling event took place the day after the lake completely mixed.

Water sampling and emission measurements were conducted primarily on cloudless days between approximately 10:30 am and 4:30 pm to capture peak emission at solar noon, and to assess the effects of increasing and decreasing solar radiation on emission. Total solar irradiance, air temperature, and other weather measurements were obtained from a weather station (Davis Instruments, Hayward, CA) installed on a floating platform moored in the center of the lake. Cosine irradiance sensors (Biospherical Instruments, San Diego, CA) installed approximately 0.2 mi from the lake measured UV radiation at 15 minute intervals for 305, 320, 340, and 380 nm with a nominal bandwidth of 8 nm, as well as total photosynthetically active radiation (400–700 nm), for the 137 duration of the experimental period.

Mercury emission was measured on five out of the six sampling dates using the dynamic flux chamber approach. The flux chamber was modeled after apparatus described by others (Kim and Lindberg, 1995; Zhang and Lindberg, 2001), and was approximately 42 cm in diameter and 20 cm in height. The chamber was constructed from acrylic and polyethylene materials with measured UV-B transmission greater than 85%. Eight holes, each approximately 4 mm in diameter, were drilled
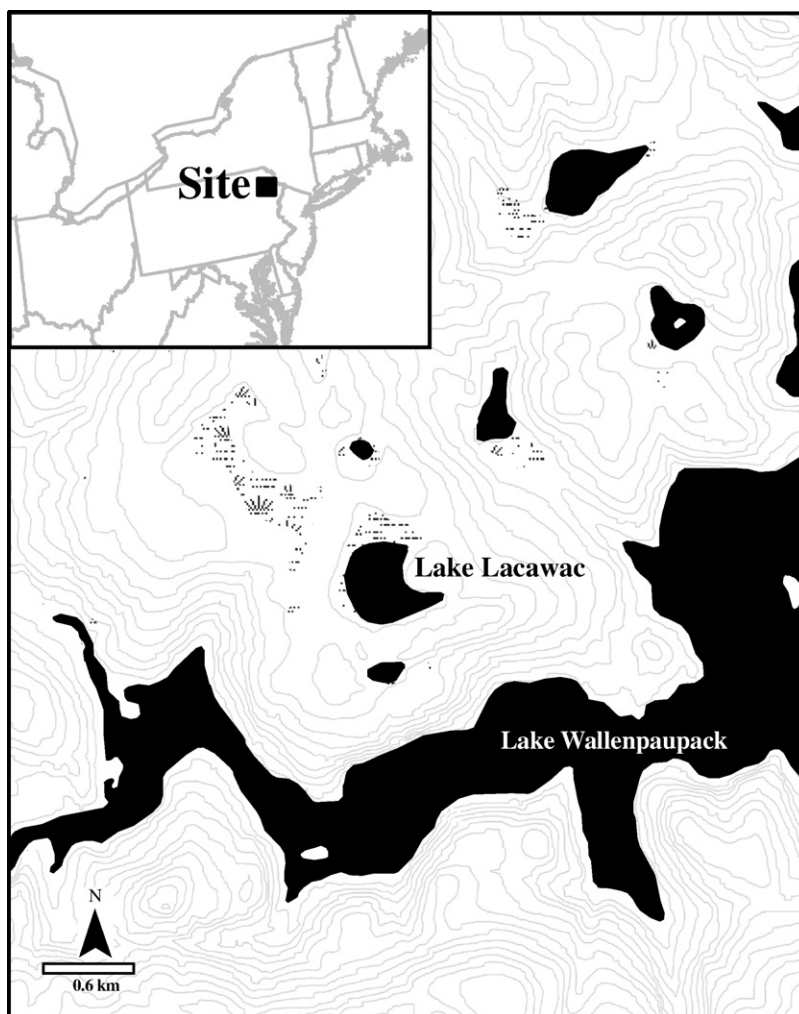
Fig. 1 – Site location map for Lake Lacawac, PA (41.3821N, 75.2916W). Wayne County (PA 41.3281N, 75.2916W).

at 45 degree intervals around the circumference of the chamber, approximately 3 cm above the water surface. The chamber was continuously pumped at a rate of 0.6 L/min during sampling. Elemental gaseous mercury concentration was determined with gold amalgamation and absorbance detection using a field portable instrument (UT-3000, Mercury Instruments, Karlsfeld, Germany). Ambient mercury concentrations were measured at the inlets of the chambers, and mercury flux rates were calculated using Eq. (1). Emission was not measured on 21 October due to technical difficulties, and data on 12 November are limited due to wind driven waves on the lake interfering with the use of the flux chamber. All flux calculations were corrected to account for flux chamber blanks, which ranged between 0.1 and 0.3 ng/m^3. The blank value represents less than 5% of the average daily flux measured at this site.

Water samples were collected using a Kemmerer bottle at 0, 2, and 8 m during every sampling event, and additional samples taken at 7, 9, and 10 m during 3 of the 6 sampling events. Samples were analyzed for major and trace elements, total dissolved mercury, and DOC using standard methods outlined below. Temperature, conductivity, pH, dissolved oxygen, and turbidity profiles were collected using a multi-parameter profiling datasonde (YSI 6600 V2-2, Yellow Springs, Ohio, USA).

Samples for mercury analysis were filtered through 0.45 μm polypropylene syringe filters into acid-cleaned 250 mL glass bottles with Teflon septa using clean techniques and oxidized with approximately 1% (v/v) bromine mono-chloride at the time of collection, with care taken to ensure that no headspace remained in the container. Field blanks using deionized water confirmed that the sample collection and filtration procedure did not add mercury to the water samples.

Water samples for ICP-MS and iron analysis were filtered using 0.45 μm polypropylene filters into acid-cleaned low density polyethylene or glass containers, respectively. Samples for ICP-MS analysis were acidified to pH 2 at the time of collection using double subboiling distilled nitric acid. DOC samples were filtered using a pre-rinsed Whatman GF/F filter into glass vials with Teflon septa, with care taken to ensure that no headspace remained in the container. Changes in DOC properties were monitored by measuring dissolved

absorbance, which reflects the degree of photobleaching and aromaticity.

2.2. Sample analysis

Mercury samples were analyzed following the methods outlined in Gill and Fitzgerald (1987). In summary, samples were sequentially reduced with hydroxylamine hydrochloride to neutralize free halogens and stannous chloride to convert all Hg^{2+} to Hg^0, and then purged with ultra-pure argon gas for 20 min, at a rate of approximately 100 mL/min. The gas stream flowed through a gold trap, which was then thermally desorbed and measured using atomic fluorescence spectroscopy (Tekran Instruments, Knoxville, TN). The fluorescence detector was calibrated using triplicate mercury vapor standard injections at 3 concentrations across the working range, with typical r^2 greater than 0.995. Recovery from liquid samples was measured to be greater than 90%, as determined using an aqueous mercury standard (High Purity Standards, Charleston, SC, USA) at dilutions across the calibrated range. The absolute detection limit for this method was determined to be 2 pg, or 4 times the average system blank. The absolute detection limit is 4 times less than the lowest concentration samples used in the analysis. One sample from 12 November (9 m) was not used in the analyses because the result was only 1.6 times the detection limit.

Water sample DOC concentration was measured on a Shimadzu TOC-V (Columbia, Maryland) considering the approach outlined by Sharp et al. (1993). Optical measurements of the dissolved absorbance (ad) of DOC were made on filtered samples using a Shimadzu UV–VIS 1601 dual beam spectrophotometer (200–800 nm) and 1 cm quartz Suprasil cuvette referenced to air. DOC-specific absorbance at several UV wavelengths (305, 320, 340, and 380 nm), as well as UV-A and UV-B spectral slopes, were used as indicators of DOC photobleaching as described by Morris et al. (1995). The ratio of dissolved absorbance at 250 nm to 365 nm ($a_{d250}:a_{d365}$) was

calculated as an index of molecular size by Morris and Hargreaves (1997). Specific UV absorbance at 254 nm (SUVA), which provides a measure of DOC aromaticity, was also calculated as described by Weishaar et al. (2003).

Samples for iron speciation were analyzed spectrophotometrically (Spectronic Unicam) within 4 h of collection, following standard procedures (Eaton et al., 1995). The ratio of Fe(II) absorbance and Fe(total) absorbance was then applied to total iron concentrations measured using ICP-MS to determine the relative concentrations of Fe(II) and Fe(III) in solution. All elemental chemistry aside from mercury was determined using ICP-MS with pneumatic nebulization (ICP-MS, Thermo X-Series CCT, Winsford, UK). The ICP-MS was calibrated with six standards across the working range with typical r^2 values of 0.999. Total analytical uncertainties were calculated at less than 5% for ICP-MS measurements.

2.3. Data analysis

Data analyses were performed using Statgraphics Centurion (StatPoint, Inc.) and SigmaPlot (SPSS). Single and multiple regression analyses were conducted to identify relationships between J_{Hg}, dissolved mercury, and other water chemical and physical characteristics. Pearson's correlation coefficients (r) were used in conjunction with ANOVA tests to evaluate the significance of these relationships. The difference between regression slopes and intercepts for data from different days was assessed using ANCOVA.

3. Results

Lake stratification remained stable at the end of August, with water temperatures of approximately 24 °C in the top 1 m, and the top of the thermocline positioned at 2.5 m depth. A decline in overnight air temperatures and increased wind speeds just
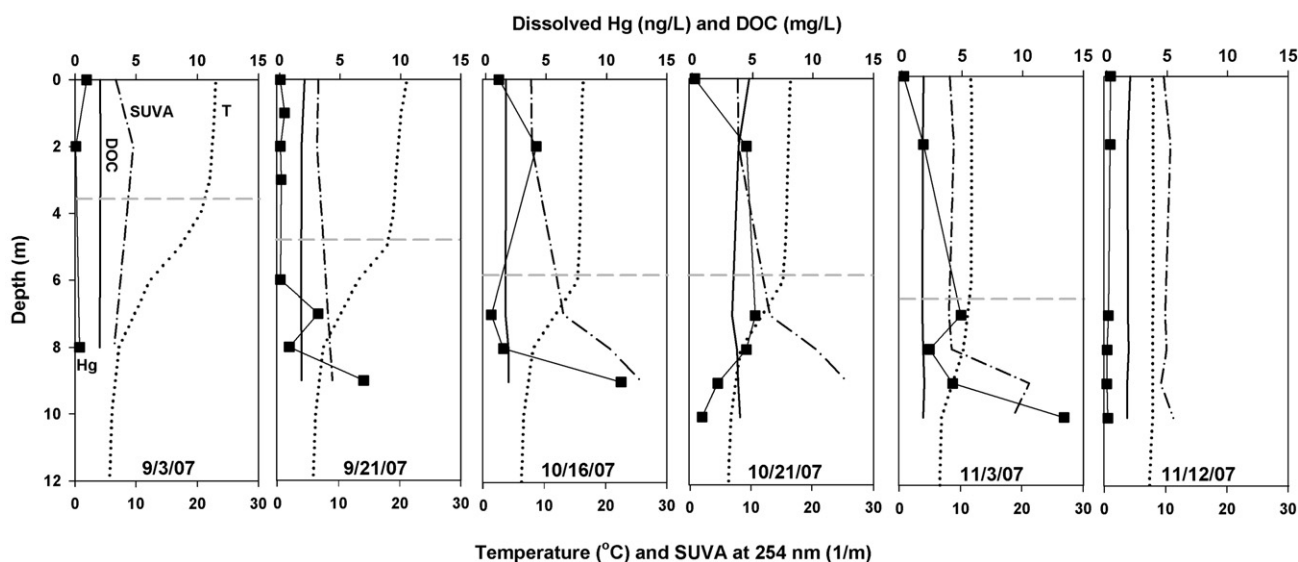

Fig. 2 – Aqueous chemistry profiles between 3 September and 12 November. Total dissolved mercury concentrations are indicated by the solid black line and black squares, and enrichment was typically observed below the thermocline (indicated by horizontal dashed grey line). DOC concentration was nearly constant with depth (solid black line). Dotted line represents temperature (°C), and dash–dotted line represents SUVA (1/m), and both correspond to the bottom axis.

| Table 1 – Raw water chemistry data and selected DOC optical measures, presented to 2 significant figures								
Date	Depth (m)	Temp (deg C)	Hg (ng/L)	Mn (µg/L)	Fe (µg/L)	DOC (mg/L)	SUVA254	S_{UVB}
9/3/2007	0.0	23.0	0.9	8	40	4.1	6.7	0.0210
	2.0	22.0	n.d.	8	43	4.2	9.5	0.0150
	8.0	7.2	0.3	1200	280	4.1	6.4	0.0210
9/21/2007	0.0	21.0	n.d.	7	53	4.4	6.7	0.0190
	1.0	20.0	0.4	9	39	NR	NR	NR
	2.0	20.0	n.d.	7	44	3.9	6.5	0.0210
	3.0	19.0	0.1	7	42	4.2	7.1	0.0190
	6.0	13.0	n.d.	17	55	4.2	5.8	0.0220
	7.0	8.6	3.2	250	260	3.9	8.3	0.0160
	8.0	7.5	0.8	550	220	3.9	8.6	0.0160
	9.0	6.9	6.9	620	630	3.9	9.0	0.0170
10/16/2007	0.0	16.0	1.0	68	71	3.7	7.5	0.0190
	2.0	16.0	4.1	72	71	3.7	8.2	0.0180
	7.0	7.9	0.4	80	74	3.6	7.6	0.0190
	8.0	6.9	1.4	250	120	4.1	8.5	0.0180
	9.0	6.5	11.0	1200	2600	4.1	22.0	0.0110
10/21/2007	0.0	16.0	n.d.	80	93	4.7	7.8	0.0180
	2.0	16.0	4.3	75	110	3.8	8.0	0.0180
	7.0	NR	4.4	320	140	3.3	13.0	0.0140
	8.0	8.3	2.0	710	1000	3.7	21.0	0.0110
	9.0	NR	5.0	1200	2600	3.8	26.0	0.0092
	10.0	6.7	0.7	1200	4200	4.0	1.3	0.0230
11/3/2007	0.0	12.0	0.1	180	200	3.9	8.2	0.0170
	2.0	12.0	1.7	190	180	3.8	8.9	0.0170
	7.0	NR	4.7	190	190	3.7	8.1	0.0170
	8.0	10.0	2.1	180	180	3.8	8.6	0.0160
	9.0	NR	4.0	870	2600	4.1	21.0	0.0110
	10.0	6.9	13.0	700	2200	3.9	19.0	0.0100
11/12/2007	0.0	7.9	0.3	240	360	4.2	9.7	0.0160
	2.0	8.0	0.3	190	230	3.8	11.0	0.0150
	7.0	7.7	0.1	190	250	3.9	9.9	0.0150
	8.0	7.9	n.d.	200	210	3.9	10.0	0.0150
	9.0	7.7	n.d.	200	210	3.7	9.2	0.0150
	10.0	7.9	0.1	290	480	3.7	11.0	0.0140

NR indicates that the data were not recorded.
n.d. indicates that Hg was less than the detection limit of 2 pg.

prior to the first sampling event, between 31 August and 2 September, resulted in the deepening of the thermocline to approximately 4 m. The thermocline remained at approximately this position until mid-October, when a partial mixing event lowered the thermocline from 4.5 m to 7 m over the course of 4 days due to a decline in air temperature. Air and water temperatures continued to decrease until the surface water temperature reached 8 °C and the lake completely mixed between 11 and 13 November. The depth to the top of the thermocline is shown on Fig. 2, and water temperature data for all sampling events are presented in Table 1.

Mercury emission rates ranged between 0.14 and 20.95 ng/m² h during the measurement period, with each day's emission rate tracking with incoming solar radiation (Fig. 3). The net mercury emission produced for each unit of incoming solar radiation was quantified by plotting cumulative mercury flux vs. cumulative solar radiation for each day (Fig. 4). This plot minimizes the effect of any potential lag between production of DGM and emission of the reduced mercury (due to diffusion, short-duration variations in wind speed, or other factors) so that the underlying DGM production rate can be visualized. For each date, cumulative mercury emission demonstrated a strong positive correlation with cumulative total solar radiation ($r^2 = 0.87$ to 0.99, $p < 0.007$ in all cases).
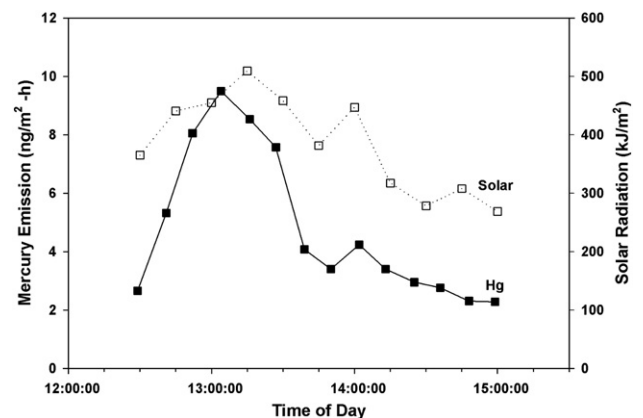
Fig. 3 – Solar radiation (open squares) and mercury emission (filled squares) for 16 October. Emission rates generally track irradiance.
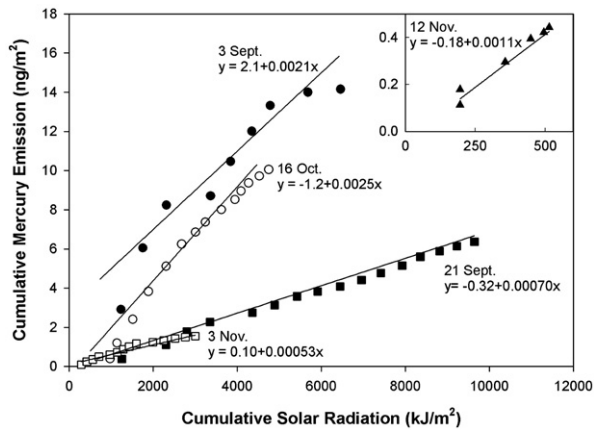
Fig. 4 – Cumulative mercury emission vs. cumulative solar radiation for all sampling dates. Regression explains between 94 and 99% of variance at $p < = 0.0002$. Data from 12 November are lower than other dates and have been inset for visibility.

Mercury emission also correlated with UV-A and UV-B wavebands ($r^2 = 0.89$ to 0.99, $p < 0.007$ in all cases), and correlation coefficients for the UV wavebands were not significantly different than those for total solar radiation ($p > 0.28$).

The slopes of the regressions (M) depicted in Fig. 4 indicate the amount of mercury emitted per kJ of incident solar radiation per unit area (termed apparent photoefficiency in this study), with differences in the slopes suggesting differences in the overall balance between mercury oxidation and reduction reactions (i.e. lower slope is indicative of less net reduction resulting in emission). The apparent photoefficiency varied from 0.5 ng/J on 3 November to 2.5 ng/J on 16 October. Surface water mercury concentrations exerted the strongest control on the apparent photoefficiency (Fig. 5; $r^2 = 0.96$, $p = 0.003$). The remaining 4% variation that is not accounted for by surface water mercury could be due to other variables, such as windspeed, DOC concentration or optical properties, iron, or other cations. However, inclusion of additional variables using multiple regression analysis did not improve the correlation between dissolved mercury concentration and apparent photoefficiency. The residuals of the regression between apparent photoefficiency and surface water mercury concentration did not correlate with any measured parameter.

Dissolved mercury concentration profiles in the lake varied during the destratification period, with average mercury concentrations higher in the hypolimnion (7–10 m) than in the epilimnion (0–2 m) on 4 of the 6 sampling dates (Fig. 2 and Table 1). The exceptions are on 3 September, when samples were not collected below 8 m, and 12 November, following lake mixing.

Dissolved iron and manganese tended to be enriched in the hypolimnion, and were positively correlated with each other ($r^2 = 0.65$, $p < 0.0001$; Fig. 7 and Table 2). Dissolved mercury concentrations for samples from all depths showed a positive relationship with total dissolved iron concentrations ($r^2 = 0.50$; $p < 0.0001$) as well as manganese ($r^2 = 0.32$, $p = 0.006$; Fig. 7). No significant relationship was identified between dissolved

mercury concentrations and iron species (Fe(II) or Fe(III)) concentrations ($r^2 < 0.10$, $p > 0.05$). Mercury emission and apparent photoefficiency were not correlated with surface water total iron, Fe(II), Fe(III), or manganese concentrations ($r^2 > 0.45$, $p > 0.05$).

DOC concentrations did not vary substantially with depth or time (Fig. 2 and Table 1). Regression between dissolved mercury concentrations and DOC concentrations did not indicate a significant relationship ($r^2 = 0.03$, $p > 0.05$). Dissolved absorbance, including SUVA, was positively correlated with dissolved mercury concentrations ($r^2 = 0.38$, $p < 0.001$) and dissolved iron concentrations ($r^2 = 0.88$, $p < 0.001$; Fig. 7 and Table 2), but not with DOC concentrations ($r^2 = 0.02$, $p > 0.05$). Mercury concentrations demonstrated a significant negative relationship with spectral slope ($r^2 = 0.19$ and 0.31 for UVA and UVB respectively, $p < 0.01$; Table 2), which is an indicator of the degree of DOC photobleaching. These optical measures also often co-vary with one another and with iron. The molecular weight ratio $a_{d250}:a_{d365}$ was not significantly correlated with mercury concentrations ($r^2 = 0.05$, $p > 0.05$; Table 2).

Dissolved sulfide was not measured, but a sulfide odor was observed below 8 m during the 21 Sept, 16 and 21 October, and 3 November sampling events. Total suspended particulates (TSP) and particulate mercury were not measured in this study, although TSP was visually observed to be higher in the hypolimnion than the epilimnion.

4.   Discussion

Emission of mercury from the water column of lakes and rivers is strongly dependent on solar radiation, as many authors have shown (e.g. Amyot et al., 1997c; Costa and Liss, 2000; Ferrara et al., 2000). However, if emission rates were solely a function of solar radiation, mercury emission would consistently decline as total incoming solar radiation progressively decreases through the summer to autumn seasons. However, this trend was not observed (Fig. 4) and mercury emission per kJ solar radiation was higher than would be predicted on two dates in the middle of autumn, 16 October and 12 November. This finding indicates that the linear
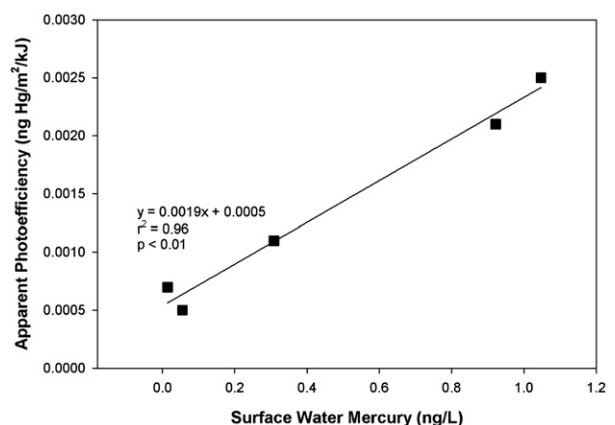
Fig. 5 – Mercury emission per kJ solar radiation vs. surface water mercury concentrations.

Table 2 – Correlation and regression statistics for single regression analyses for water chemistry at all depths

|	Mn	Fe total	Fe II	Fe III	DOC	a_{305}/DOC	a_{320}/DOC	a_{340}/DOC	a_{380}/DOC	S_{UVA}	S_{UVB}	$a_{d250}{:}a_{d365}$	$SUVA_{254}$
Hg	0.56 (34) **0.0006**	0.71 (34) **<0.0001**	0.22 (18) 0.3708	0.26 (18) 0.2923	−0.18 (33) 0.3029	0.60 (33) **0.0002**	0.60 (33) **0.0002**	0.60 (33) **0.0002**	0.59 (33) **0.0003**	−0.44 (32) **0.0123**	−0.56 (33) **0.0008**	−0.23 (33) 0.1951	0.59 (33) **0.0003**
Mn		0.81 (34) **<0.0001**	0.57 (18) **0.0136**	0.66 (18) **0.0028**	−0.05 (33) 0.7850	0.56 (33) **0.0006**	0.58 (33) **0.0004**	0.59 (33) **0.0003**	0.59 (33) **0.0003**	−0.40 (32) **0.0233**	−0.39 (33) **0.0234**	−0.22 (33) 0.2118	0.53 (33) **0.0015**
Fe total			0.51 (18) **0.0315**	0.77 (18) **0.0002**	0.02 (33) 0.9316	0.54 (33) **0.0012**	0.56 (33) **0.0007**	0.57 (33) **0.0005**	0.58 (33) **0.0004**	−0.56 (32) **0.0008**	−0.36 (33) **0.0399**	−0.26 (33) 0.1512	0.49 (33) **0.0039**
Fe II				−0.17 (18) 0.5108	0.00 (18) 0.9959	0.78 (18) **0.0001**	0.79 (18) **0.0001**	0.80 (18) **0.0001**	0.81 (18) **<0.0001**	−0.62 (17) **0.0076**	−0.70 (18) **0.0013**	−0.17 (18) 0.4990	0.77 (18) **0.0002**
Fe III					0.17 (18) 0.5117	−0.05 (18) 0.8473	−0.03 (18) 0.9081	−0.02 (18) 0.9444	−0.01 (18) 0.9707	−0.30 (17) 0.2342	0.18 (18) 0.4867	−0.21 (18) 0.4092	−0.10 (18) 0.6801
DOC						−0.16 (33) 0.3637	−0.16 (33) 0.3708	−0.16 (33) 0.3734	−0.16 (33) 0.3702	0.30 (32) 0.0927	0.26 (33) 0.1385	0.07 (33) 0.7015	−0.17 (33) 0.3468
a_{305}/DOC							0.89 (34) **<0.0001**	0.90 (34) **<0.0001**	0.61 (34) **0.0001**	0.24 (33) 0.1760	0.24 (34) 0.1664	−0.24 (34) 0.1640	1.00 (34) **<0.0001**
a_{320}/DOC								1.00 (34) **<0.0001**	0.18 (34) 0.3115	−0.24 (33) 0.1717	−0.23 (34) 0.1901	−0.21 (34) 0.2235	0.89 (34) **<0.0001**
a_{340}/DOC									0.20 (34) 0.2570	−0.22 (33) 0.2142	−0.21 (34) 0.2328	−0.22 (34) 0.2113	0.89 (34) **<0.0001**
a_{380}/DOC										0.92 (33) **<0.0001**	0.92 (34) **<0.0001**	−0.17 (34) 0.3432	0.60 (34) **0.0002**
S_{UVA}											1.00 (33) **<0.0001**	−0.08 (33) 0.6711	0.24 (33) 0.1878
S_{UVB}												−0.07 (34) 0.6803	0.23 (34) 0.1816
$a_{d250}{:}a_{d365}$													−0.23 (34) 0.1902

Values listed for each parameter are: Top = Pearson's r; middle = (number of samples); bottom = p-value from ANOVA test. Values in bold indicate significance at alpha = 0.05.

relationship observed between solar radiation and mercury emission and/or DGM concentration in many studies of diel and seasonal mercury cycles (e.g. Amyot et al., 1997a; Dill et al., 2006; Krabbenhoft et al., 1998; Zhang et al., 2006) is somewhat more complex during lake turnover.

The changes in mercury emission per unit of solar radiation observed in this study can be explained by considering surface water mercury concentrations. Changes in surface mercury concentrations explain 96% of the variation in mercury emission per unit of solar radiation ($p<0.01$; Fig. 5), with higher dissolved mercury concentrations resulting in higher mercury emissions for a given amount of solar radiation. This finding is consistent with the results of spiked lake water incubations conducted by Amyot et al. (1997b), who found a linear increase in DGM production with increasing Hg (II) concentrations. Our data indicate that lake mixing is the most likely factor that explains changes in dissolved mercury concentrations in the surface water. Mercury concentration in

surface waters (0 m) increased as a result of partial (16 October) and full (12 November) mixing events in the lake (Fig. 6), which transferred mercury from the hypolimnion to the epilimnion. The dissolved mercury concentration at the beginning of our experiment on 3 September may also have been slightly elevated due to a small partial mixing event that occurred 1 to 3 days prior to the first sampling event, when the depth of the thermocline dropped from approximately 3 to 4 m, but no mercury data from August are available to confirm this observation. Surface water mercury concentrations then decline between mixing events, potentially due to loss via emission.

In summary, if surface water mercury concentrations had remained constant throughout the mixing period then the seasonal decrease in solar radiation would cause a continuously declining emission rate. Our observations show that periodic increases in emission were observed coincident with mixing events that most likely transported mercury from the
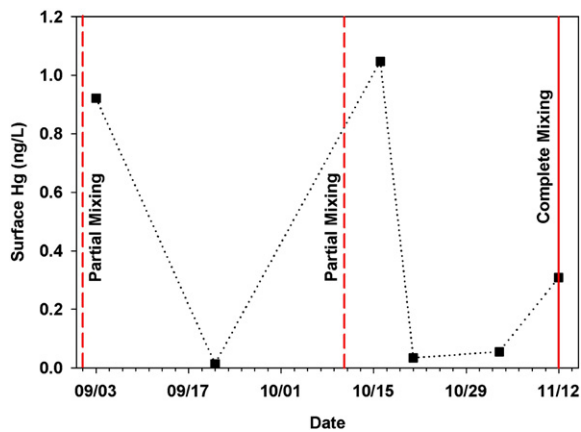
Fig. 6 – Surface water mercury concentrations over time. Minor erosion of the thermocline between 31 August and 2 September may have contributed to the high mercury concentration observed on 3 September. A partial mixing event between 13 and 16 October resulted in increased dissolved Hg concentration. Mercury concentrations increased again on 12 November when the lake mixed completely.

hypolimnion up into the epilimnion. If continuous monitoring over long time periods were possible, it is likely that periodic peaks in mercury emission would be observed throughout the

autumn corresponding to partial mixing events as the thermocline erodes.

4.1. Mercury interactions with iron, DOC, and sulfide

The addition of Fe (III) (1 to 30 μM) to natural water samples can enhance production of DGM, and indicates that inputs of iron to natural waters may enhance mercury emission (Zhang and Lindberg, 2001). Surface water total iron concentrations increased throughout the measurement period in this study (~0.72 to 6.4 μM), as did Fe(III) concentrations, but neither mercury emission rates nor apparent photoefficiency demonstrated a corresponding increase ($r^2 < 0.26$, $p > 0.05$). Mercury, iron and manganese were enriched in the hypolimnion relative to epilimnetic concentrations, and were positively correlated to each other (Fig. 7B and C), suggesting that these elements are likely influenced by similar in-lake processes. Other studies have also suggested that mercury transport in the water column may be linked to iron or manganese cycles (Chadwick et al., 2006). Although total iron was correlated with dissolved mercury concentrations at all depths, iron speciation does not appear to influence mercury transport in this lake. No significant relationship was observed between Fe(II) or Fe(III) concentrations and dissolved mercury concentrations or mercury emission, in contrast to the findings of Zhang and Lindberg (2001).
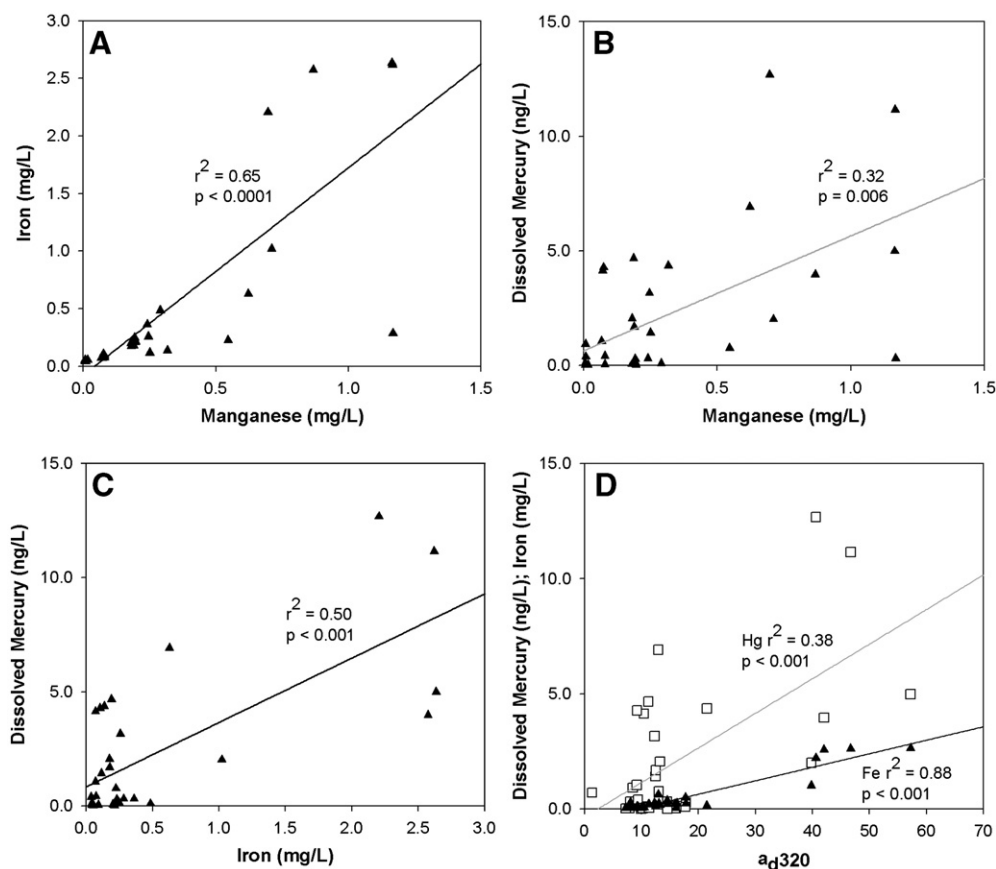
Fig. 7 – Relationships between A) dissolved iron and manganese concentrations; dissolved mercury as a function of B) manganese concentrations; C) toral iron; and D) mercury and iron as a function of dissolved UV absorbance at 320 nm, for all water depths. Regressions are significant at p-values indicated on each graph.

Although many studies have identified a significant role for DOC in the formation of Hg^0 (Garcia et al., 2005; Tseng et al., 2004; Watras et al., 1995), no relationship was observed between DOC concentration and dissolved mercury concentration or mercury emission rate in this study. It is likely that the range of DOC concentrations measured in this study (3.3 to 4.7 mg/L) was not large enough to produce a statistically significant effect. Dissolved absorbance measures changed throughout the observation period. Dissolved absorbance was strongly correlated with iron ($r^2=0.88$), consistent with other reports for this lake (Maloney et al., 2005), but was not significantly correlated with DOC ($r^2=0.02$). Higher dissolved absorbance measurements correlated with increased concentrations of dissolved mercury, providing additional evidence that iron may play a role in mercury transport within Lake Lacawac. Other studies have identified the degree of DOC aromaticity as important for mercury–DOC interactions and mercury speciation (Aiken et al., 2001; Garcia et al., 2005), and several optical measures of DOC chemical characteristics and photobleaching showed significant correlations with dissolved mercury concentrations. However, the role of DOC optical properties for mercury cycling in Lake Lacawac is less clear due to the confounding relationship between iron and dissolved absorbance.

It is also possible that other ligands such sulfide are as, or more, important for mercury transport and speciation in this lake. Sulfide complexes can play an important role in mercury cycling and speciation (e.g. Benoit et al., 1999; Reddy and Aiken, 2001). Sulfide was not measured in this study, though a sulfide odor was observed in the hypolimnion on four of the sampling dates. Assuming that the sulfide concentration was at least the minimum perceptible to humans (approximately 1.5×10^{-5} M hydrogen sulfide), speciation modeling using PhreeqC Interactive 2.15.0 (Parkhurst and Appelo, 1999) indicates that essentially all dissolved mercury in the hypolimnion is present as various sulfide complexes. Sulfide concentrations greater than 10^{-10} M will dominate mercury speciation (Reddy and Aiken, 2001), so the lack of a significant relationship between other ligands and dissolved mercury concentrations in the hypolimnion was likely the result of sulfide being the primary ligand binding mercury. Speciation modeling also indicates that hypolimnetic waters are oversaturated with respect to both cinnabar and metacinnabar (saturation index>6.2). The speciation model (Parkhurst and Appelo, 1999) is consistent with laboratory experiments that demonstrated inhibition of metacinnabar precipitation at the circumneutral pH and DOC concentrations (average=3.9 mg/L) observed in this lake (Ravichandran et al., 1999).

4.2. Conclusions

This study reaffirms the predominance of solar radiation in controlling mercury emission from waterbodies. In addition, our data indicate that surface water mercury concentration may also influence mercury emission rates. Mercury emission from lakes may increase during seasonal mixing as mercury is transported from the hypolimnion up to the epilimnion. Diel variability in solar radiation still appears to control the daily pattern of emission, though each day's emission appears to be scaled by the surface water mercury concentration. Epilimnetic mercury concentrations increased during mixing, and then decreased via emission to the atmosphere. Dissolved mercury concentrations throughout the water column were lower after lake mixing, suggesting that emission during mixing is a significant pathway that removes mercury from lake ecosystems.

REFERENCES

Aiken G, Reddy M, Ravichandran M, Ryan J. Interactions between dissolved organic matter and mercury. Abst Papers Am Chem Soc 2001;221:U451-U451.

Amyot M, Gill GA, Morel FMM. Production and loss of dissolved gaseous mercury in coastal seawater. Environ Sci Technol 1997a;31:3606–11.

Amyot M, Lean D, Mierle G. Photochemical formation of volatile mercury in Arctic lakes. Environ Toxicol Chem 1997b;16:2054–63.

Amyot M, Mierle G, Lean D, McQueen DJ. Effect of solar radiation on the formation of dissolved gaseous mercury in temperate lakes. Geochim Cosmochim Acta 1997c;61:975–87.

Benoit JM, Gilmour CC, Mason RP, Heyes A. Sulfide controls on mercury speciation and bioavailability to methylating bacteria in sediment pore waters. Environ Sci Technol 1999;33:951–7.

Carpi A, Lindberg SE. Application of a Teflon (TM) dynamic flux chamber for quantifying soil mercury flux: tests and results over background soil. Atmos Environ 1998;32:873–82.

Chadwick SP, Babiarz CL, Hurley JP, Armstrong DE. Influences of iron, manganese, and dissolved organic carbon on the hypolimnetic cycling of amended mercury. Sci Total Environ 2006;368:177–88.

Costa M, Liss P. Photoreduction and evolution of mercury from seawater. Sci Total Environ 2000;261:125–35.

Dill C, Kuiken T, Zhang H, Ensor M. Diurnal variation of dissolved gaseous mercury (DGM) levels in a southern reservoir lake (Tennessee, USA) in relation to solar radiation. Sci Total Environ 2006;357:176–93.

Eaton AD, Clesceri LS, Greenberg AE. Standard methods for the examination of water and wastewater. Washington, D.C.: American Public Health Association; 1995. p. 1325.

Ferrara R, Mazzolai B, Lanzillotta E, Nucaro E, Pirrone N. Temporal trends in gaseous mercury evasion from the Mediterranean seawaters. Sci Total Environ 2000;259:183–90.

Garcia E, Amyot M, Ariya PA. Relationship between DOC photochemistry and mercury redox transformations in temperate lakes and wetlands. Geochim Cosmochim Acta 2005;69:1917–24.

Gill GA, Fitzgerald WF. Picomolar mercury measurements in seawater and other materials using stannous chloride reduction and 2-stage gold amalgamation with gas-phase detection. Mar Chem 1987;20:227–43.

Haitzer M, Aiken GR, Ryan JN. Binding of mercury(II) to aquatic humic substances: influence of pH and source of humic substances. Environ Sci Technol 2003;37:2436–41.

Herrin RT, Lathrop RC, Gorski PR, Andren AW. Hypolimnetic methylmercury and its uptake by plankton during fall

destratification: a key entry point of mercury into lake food chains? Limnol. Oceanography 1998;43:1476–86.

Kim KH, Lindberg SE. Design and initial tests of a dynamic enclosure chamber for measurements of vapor-phase mercury fluxes over soils. Water, Air, Soil Pollut 1995;80:1059–68.

Krabbenhoft DP, Hurley JP, Olson ML, Cleckner LB. Diel variability of mercury phase and species distributions in the Florida Everglades. Biogeochemistry 1998;40:311–25.

Lalonde JD, Amyot M, Kraepiel AML, Morel FMM. Photooxidation of Hg(0) in artificial and natural waters. Environ Sci Technol 2001;35:1367–72.

Lindberg SE, Hanson PJ, Meyers TP, Kim KH. Air/surface exchange of mercury vapor over forests — the need for a reassessment of continental biogenic emissions. Atmos Environ 1998;32:895–908.

Maloney KO, Morris DP, Moses CO, Osburn CL. The role of iron and dissolved organic carbon in the absorption of ultraviolet radiation in humic lake water. Biogeochemistry 2005;75:393–407.

Morel FMM, Kraepiel AML, Amyot M. The chemical cycle and bioaccumulation of mercury. Annu Rev Ecol Syst 1998;29:543–66.

Morris DP, Hargreaves BR. The role of photochemical degradation of dissolved organic carbon in regulating the UV transparency of three lakes on the Pocono Plateau. Limnol Oceanogr 1997;42:239–49.

Morris DP, Zagarese H, Williamson CE, Balseiro EG, Hargreaves BR, Modenutti B, et al. The role of solar UV radiation in lakes and the role of dissolved organic carbon. Limnol Oceanogr 1995;40:1381–91.

Parkhurst DL, Appelo CAJ. User's guide to PHREEQC (version 2)—a computer program for speciation, batch-reaction, one-dimensional transport and inverse geochemical calculations. Water-Resources Invest Rep 1999:99-4259.

Ravichandran M, Aiken GR, Ryan JN, Reddy MM. Inhibition of precipitation and aggregation of metacinnabar (mercuric sulfide) by dissolved organic matter isolated from the Florida Everglades. Environ Sci Technol 1999;33:1418–23.

Reddy MM, Aiken GR. Fulvic acid-sulfide ion competition for mercury ion binding in the Florida Everglades. Water, Air, Soil Pollut 2001;132:89-104.

Sharp JH, Suzuki Y, Munday WL. A comparison of dissolved organic-carbon in North-Atlantic Ocean nearshore waters by high-temperature combustion and wet chemical oxidation. Mar Chem 1993;41:253–9.

Slotton DG, Reuter JE, Goldman CR. Mercury uptake patterns of biota in a seasonally anoxic northern California reservoir. Water, Air, Soil Pollut 1995;80:841–50.

Tseng CM, Lamborg C, Fitzgerald WF, Engstrom DR. Cycling of dissolved elemental mercury in Arctic Alaskan lakes. Geochim Cosmochim Acta 2004;68:1173–84.

Vandal GM, Mason RP, Fitzgerald WF. Cycling of volatile mercury in temperate lakes. Water, Air, Soil Pollut 1991;56:791–803.

Watras CJ, Bloom NS. The vertical distribution of mercury species in Wisconsin lakes: accumulation in plankton layers. In: Watras CJ, Huckabee JW, editors. Mercury pollution: integration and synthesis. Lewis; 1994. p. 137–52.

Watras CJ, Morrison KA, Host JS, Bloom NS. Concentration of mercury species in relationship to other site-specific factors in the surface waters of northern Wisconsin lakes. Limnol Oceanogr 1995;40:556–65.

Weishaar JL, Aiken GR, Bergamaschi BA, Fram MS, Fujii R, Mopper K. Evaluation of specific ultraviolet absorbance as an indicator of the chemical composition and reactivity of dissolved organic carbon. Environ Sci Technol 2003;37:4702–8.

Zhang H, Lindberg SE. Sunlight and iron(III)-induced photochemical production of dissolved gaseous mercury in freshwater. Environ. Sci. Technol. 2001;35:928–35.

Zhang HH, Poissant L, Xu XH, Pilote M, Beauvais C, Amyot M, et al. Air–water gas exchange of mercury in the Bay Saint Francois wetlands: observation and model parameterization. J Geophys Res Atmos 2006;111.